Journal of Chromatography A, 1288 (2013) 54–62

Contents lists available at SciVerse ScienceDirect

Journal of Chromatography A

journal homepage: www.elsevier.com/locate/chroma

Characterization of oxidized phospholipids in oxidatively modified low density lipoproteins by nanoflow liquid chromatography–tandem mass spectrometry

Ju Yong Lee[a], Sangsoo Lim[a], Sungha Park[b], Myeong Hee Moon[a,*]

[a] Department of Chemistry, Yonsei University, Seoul 120-749, South Korea
[b] Division of Cardiology, Yonsei University College of Medicine, Seoul 120-752, South Korea

ARTICLE INFO

Article history:
Received 7 January 2013
Received in revised form 15 February 2013
Accepted 27 February 2013
Available online 13 March 2013

Keywords:
Phospholipids
Oxidized phospholipid
LDL
Ox-LDL
LC–ESI–MS^n
Tandem mass spectrometry

ABSTRACT

Oxidized low density lipoproteins (Ox-LDLs) have an important role in the development of age-related vascular disease, such as atherosclerosis. Ox-LDLs are defined as oxidatively modified LDLs in the blood by enzymatic or non-enzymatic oxidation of phospholipids (PLs). For the characterization of Ox-LDLs at molecular level, oxidation patterns of oxidized PL (Ox-PL) products were systematically examined with standard PL molecules (16:0/22:6-PC, 18:0/22:6-PA, and 18:0/22:6-PG), by the formation of bilayer vesicles of each standard, followed by oxidation of PL vesicles using a Cu^{2+} solution. This oxidative modification was applied to LDL standard materials. Nanoflow liquid chromatography–electrospray ionization–tandem mass spectrometry (nLC–ESI–MS/MS) analysis of the extracted PL mixtures resulted in the identification of 276 PLs both in the modified and non-modified LDL, including 139 Ox-PL species. Examination of the identified PL species from the standard LDL before and after oxidation supported the postulate that the specific location of an acyl chain of LPL can be exchanged between the sn-1 and -2 positions. This exchange occurs when the neighboring acyl chain is cleaved during oxidation and the polar head group of PL molecules can be dissociated to form PA molecules that result in the formation of various Ox-PA products. This study demonstrates that nLC–ESI–MS^n can be utilized for the separation and structural characterization of complicated Ox-PL mixtures, including long chain products with hydroxylation or hydroperoxylation at an unsaturated acyl chain, and short chain products from the cleavage of unsaturated fatty acyl chains to form lysophospholipids (LPLs) or the truncation of an acyl chain into a shorter chain terminated with aldehyde or carboxylic acid.

1. Introduction

Medical interest in the oxidized low density lipoproteins (Ox-LDLs) began when Ox-LDL were shown to play a major role in the development and progression of age-related chronic diseases, atherosclerosis, and inflammation [1–4]. Oxidation of LDL is a complex process promoted by either enzymatic (lipoxygenase or myeloperoxidase) or non-enzymatic reactions (iron- or copper-mediated oxidation) and primarily occurs in unsaturated fatty acid chains of phospholipids (PLs) contained in LDLs. It has been reported that oxidized phospholipids (Ox-PLs) can activate the receptor for a platelet-activating factor which induces platelet-aggregation [5]. It also plays a role in the signaling inflammatory response [6], and induces physical change in biological membranes leading to variations in fluidity and acyl packing [7–9]. In addition, oxidized phosphatidylcholine (Ox-PC) products are reported to be directly involved with atherosclerosis [4,10]. Therefore, it is very important to understand the oxidative modification of LDLs at the molecular level by the comprehensive analysis of Ox-PL products.

Oxidation of the PL molecule usually occurs by abstraction of a hydrogen atom from a bis-allylic methylene of a polyunsaturated fatty acid (more preferable than a single unsaturated chain) in PL either *via* an inorganic reactive oxygen species (ROS) or enzymatic oxidation. The hydrogen abstraction results in the delocalization of a radical around the neighboring C=C bonds, followed by oxygen insertion to generate a hydroperoxy radical. The hydroperoxy radical is further reduced to form PL hydroperoxide. However, the PL hydroperoxide is unstable and is further reduced to generate stable PL hydroxide or it decomposes to yield truncated oxidized lipids containing terminal carbonyl or hydroxyl groups [11,12].

Therefore, oxidation of PLs leads to a huge number of structurally diverse products categorized as follows: (1) long-chain products that preserve the PL skeleton with hydroxy, keto, hydroperoxy, or hypohalous groups on the sn-2 unsaturated fatty acid; (2) short-chain (or truncated) products that are formed

* Corresponding author at: Department of Chemistry, Yonsei University, Seoul 120-749, South Korea. Tel.: +82 2 2123 5634; fax: +82 2 364 7050.
E-mail addresses: mhmoon@yonsei.ac.kr, mhmoon@hotmail.com (M.H. Moon).

0021-9673/$ – see front matter © 2013 Elsevier B.V. All rights reserved.
http://dx.doi.org/10.1016/j.chroma.2013.02.086

by cleavage of unsaturated fatty acyl chains, such as aldehydes, (keto)hydroxy-aldehydes, carboxylic acids or lysophospholipids (LPLs); and (3) PL adducts formed between Ox-PL products and carbonyls or amino groups in nearby peptides or proteins [11].

Because of the potential increase in biological activity of the oxidized or oxidatively fragmented PLs, which are relatively present in low concentration, when compared to intact PLs, the comprehensive analysis of complex Ox-PLs remains a challenging task. Recent advances in mass spectrometry (MS) using the electrospray ionization (ESI) method have facilitated the screening of intact PLs [13,14] and Ox-PCs obtained from either PC vesicles treated with an external peroxidation reaction in the presence of Fe^{2+} or Cu^{2+} [15–17] or from oxidatively modified LDL [10]. With the use of collision-induced dissociation (CID) by ESI–MS/MS, It was reported that by using low-energy collision induced dissociation tandem mass spectrometry, it was possible to characterize the molecular structure of long-chain products from Ox-PC vesicles by deciphering the product ion spectra [18,19]. The structural complexity of Ox-PL products requires separation by high performance liquid chromatography (HPLC) before identifying the analyte by using ESI–MS or ESI–MS/MS, as ion suppression from intact more abundant PLs can be minimized and accordingly isobaric species of Ox-PLs can be differentiated.

LC–ESI–MS has been utilized for the separation and detection of intact Ox-PCs from oxidized PC vesicles [20,21], oxidatively stressed cells [22], and atherosclerotic plaques [23], however detailed structural determination Ox-PL species in these works was not supported by distinguished patterns of CID spectra. LC–ESI–MS/MS has expanded the scope of analysis by obtaining far more comprehensive information on the location of the acyl chain, hydroxylation and hydroperoxylation sites and partial cleavage of acyl chains [24–26]. While a number of studies have been performed to elucidate the structure of oxidized products, most of them were focused on the examination of Ox-PCs or oxidized phosphatidylethanolamines (Ox-PEs) with the use of conventional or microbore HPLC columns.

This study demonstrates for the first time that by using nLC–ESI–MS^n various Ox-PL species including isobaric species from oxidatively modified LDL can be separated and their molecular structures were determined systematically from CID patterns. Recently, nLC–ESI–MS/MS was employed to enhance the analysis of intact PL species in urine samples of patients with breast cancer and prostate cancer [27,28], and high density lipoprotein (HDL) and LDL that were size-sorted by flow field-flow fractionation [29]. For the systematic analysis of different Ox-PL patterns, bilayer vesicles were individually prepared with each PL standard (18:0/22:6-PS, 18:0/22:6-PG, and 16:0/22:6-PC) and oxidized using a Cu^{2+} solution. The cleavage patterns and oxidative modification of the resulting Ox-PL species were determined by nLC–ESI–MS^n and the fragment ion information of Ox-PL species were incorporated into the library files to be utilized with LiPilot, the computational algorithm for PL identification developed in our laboratory [30], for the identification of the Ox-PL species of an oxidatively modified LDL sample.

2. Materials and method

2.1. Materials

Seventeen lipid standards (5 LPL species and 12 PL species: 12:0-LPG (lysophosphatidylglycerol), 18:0-LPS (lysophosphatidylserine), 14:0-LPE (lysophosphatidylethanolamine), 12:0-LPC, 14:0-LPE, 12:0/12:0-PG, 14:0/14:0-PS, 16:0/18:2-PI (phosphatidylinositol), 12:0/12:0-PA (phosphatidic acid), 18:0/22:6-PA, 18:0/22:6-PG, 12:0/12:0-PC, 12:0/12:0-PE, 14:0/14:0-PE, 16:0/14:0-PC, 20:0/20:0-PC, 16:0/22:6-PC) were purchased from Avanti Polar Lipid, Inc. (Alabaster, AL, USA). Each standard contained in a solvent mixture (1:3:4 (v/v) H_2O:$CHCl_3$:CH_3OH) was diluted with CH_3CN/CH_3OH (1:9, v/v) to a concentration of 1 pmol/μL for nLC–ESI–MS–MS. One hundred microliters of a standard LDL purchased from Sigma-Aldrich Co. (St. Louis, MO, USA) was washed with 300 μL PBS buffer (pH = 7.5) and centrifuged (7000 × *g*, 10 min) ten times to remove the EDTA contained in the LDL standard solution. The final volume of the standard LDL was adjusted to 100 μL (5.1 mg/mL) and stored at 4 °C for oxidation.

2.2. Oxidation of std. phospholipids and std. LDL

Three different phospholipid vesicles (16:0/22:6-PC, 18:0/22:6-PG and 18:0/22:6-PA) were prepared individually. Preparation of bilayer vesicles of each PL standard is as follows. Each PL standard (1 mg) was dissolved in 10 mL $CHCl_3$ to form phospholipid unilamellar vesicles by extrusion. Chloroform in each flask was removed by a rotary evaporator under N_2 gas, resulting in a thin lipid film inside the flask. The film was hydrated with 2 mL PBS buffer (0.01 M phosphate buffer and 150 mM NaCl at pH 7.5) to a final concentration of 10 mg/mL. The mixture was vortexed and extruded at 40 °C using a mini-extruder from Avanti Polar Lipids, Inc. with polycarbonate membranes (100-nm pore size) to produce uniform phospholipid vesicles. For oxidative modification of PL vesicles and of standard LDL, the "*in vitro* oxidation method" [31] was slightly modified in this experiment. For oxidation, 100 μL of 10 μM $CuSO_4$ was added to 100 μL of each vesicle sample and standard LDL. The mixtures were stored at 37 °C under two different periods (1 and 2 h). To quench the oxidation reaction, 0.9 mg EDTA was added to the mixture.

For the extraction of Ox-PLs, a slightly modified Folch method was utilized. The oxidized mixtures were mixed with 50 μL MeOH and 200 μL chloroform, vortexed for 5 min., and centrifuged at 2000 × *g* for 5 min to separate distinct organic layers. The lower organic layer was stored for later use and the upper layer was removed, mixed with 100 μL chloroform, vortexed, and centrifuged again. The lower phase was mixed with the previously stored organic layer and the mixture was dried in a vacuum centrifuge from Ilshin Biobase Co. (Yangju, Korea), and dissolved in chloroform. Dissolved lipids were diluted in CH_3OH:CH_3CN (90:10, v/v) to a final concentration of 5 μg/μL for nLC–ESI–MS/MS analysis in a negative ion mode, and 10 μg/μL in a positive ion mode. The injection volume was 1 μL for each run.

2.3. Nanoflow LC–ESI–MS^n

A model 1260 Infinity Capillary Pump system equipped with an autosampler from Agilent Technologies (Palo Alto, CA, USA) was coupled with a LTQ Velos ion trap mass spectrometer from Thermo Finnigan (San Jose, CA, USA) to separate and identify Ox-PLs. The analytical column was prepared in the laboratory by packing Watchers® ODS-P C18 resin (100 Å, diameter 3 μm) from ISU Industry Co. (Seoul, Korea) in a silica capillary (75-μm I.D., 360-μm O.D., and 7-cm length) from Polymicro Technologies, LLC (Phoenix, AZ, USA). Before packing the column, one end of a capillary column was pulled by flame to make a sharp self-emitter for ESI, and then was packed with a methanol slurry of the C18 resin with helium gas under 1000 psi. After packing, the opposite end (column inlet) was connected to an in-line filter to prevent the beads from spilling backward by back pressure. The capillary column was connected to a pump by a PEEK microcross from Upchurch Scientific (Oak Harbor, WA, USA) and the two other remaining ports of the microcross were used for Pt wire as an electrical support and the on-off valve for a switch between split and injection modes, respectively. The on-off valve was closed while loading the sample,

but open in split mode. The sample was loaded into the analytical column at a flow rate of 500 nL/min from the pump. During LC runs, the pump delivered solvent at a flow rate of 10 μL/min, but only 500 nL/min was delivered to the analytical column with the rest of the flow vented with the split valve. The flow rate was controlled by varying the length of a capillary (20-μm I.D., 360-μm O.D.) at the end of the split valve.

The mobile phase A of the binary gradient LC system was H_2O:CH_3CN (90:10, v/v) and mobile phase B was composed of CH_3CN:CH_3OH:isopropanol (20:20:60, v/v). Ionization modifiers added to the mobile phase solutions were 0.1% formic acid in the positive ion mode and 0.05% ammonium hydroxide in the negative ion mode. All of the HPLC grade solvents were purchased from J.T. Baker (Phillipsburg, NJ, USA). After loading the sample into the column, the mobile phase B was increased to 50% from 0% in 1 minute, slowly increased to 90% over 29 min, ramped again to 100% in 1 min, and maintained for 10 min in the negative ion mode. In the positive ion mode, solvent B was ramped to 80% in 1 min, increased to 90% in 1 min again, and linearly increased to 100% over 24 min.

During MS analysis, 3 kV was applied to nebulize the sample for ESI. The mass ranges for the precursor MS scan were 430–950 amu for the negative ion mode and 420–950 amu for the positive ion mode. For tandem MS experiments, data dependent CID was used. The isolation width for the CID was 1 amu and the normalized collision energies were 40% and 45% for the negative and positive ion modes, respectively. From the observed patterns of fragment ions of Ox-PL products obtained by nLC–ESI–MS–MS, library files of possible Ox-PL species to be used for LiPilot [30], a computer software built in-house for the identification of the PL structure from CID spectra, were generated for the automatic search of Ox-PL species of oxidatively modified LDL particles. The searched results by LiPilot, were manually examined for validity.

3. Results and discussion

Oxidative modification patterns of PL species were studied by nLC–ESI–MS/MS analysis of Ox-PLs that were obtained by oxidizing PL vesicles with the $CuSO_4$ solution. It is essential to separate the Ox-PL species prior to MS analysis because of their complexity. Fig. 1a shows a typical separation of eight different PL standard mixtures by the nLC–ESI–MS/MS method utilized in this study. This figure illustrates that the PL molecules with different head groups and different chain lengths, can be readily resolved. In addition the respective regioisomers 1a and 1b for lyso/14:0-PG (phosphatidylglycerol) and 14:0/lyso-PG, can be well separated. The run condition of nLC–ESI–MS/MS in Fig. 1a was utilized for the separation of oxidized products of phosphatidic acid (PA) in which PA vesicles were made using 18:0/22:6-PA standards. Fig. 1b is the base peak chromatogram (BPC) of Ox-PA mixtures produced after the oxidation of 18:0/22:6-PA standard, representing a number of oxidized species eluted between 15 and 30 min along with a few species having relatively low peak intensity (the intensity of the chromatogram between 20 and 30 min was enlarged 20-fold). Peak #8 in Fig. 1b was the un-oxidized 18:0/22:6-PA standard but it was relatively broad and distorted, showing an overloading of original 18:0/22:6-PA with some Ox-PA species since it was injected with 6 μg of the oxidized mixtures to detect as many as the Ox-PA species of relatively low concentration. Identification of molecular structure of each Ox-PA species in Fig. 1b will be explained later. However, Fig. 1c is the BPC of Ox-PG products oxidized from the 18:0/22:6-PG standard (peak #17 for the un-oxidized 18:0/22:6-PG), showing relatively sharp peaks for most Ox-PG molecules. Peaks # 14-16 were not completely resolved due to the similarity in molecular structure of isobaric Ox-PG species which will be explained later.

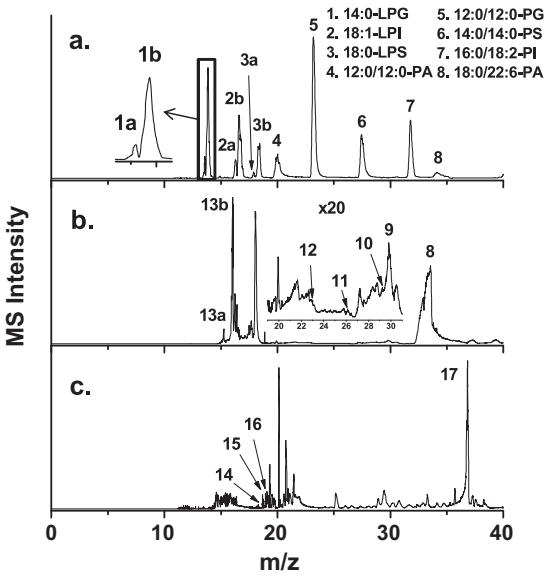

Fig. 1. Base peak chromatograms (BPCs) of (a) eight PL standards, (b) Ox-PA species obtained from oxidative modification of 18:0/22:6-PA standards (peak #18), and (c) Ox-PG species from 18:0/22:6-PG (peak #17) at the negative ion mode of nLC–ESI–MS/MS.

From the data-dependent CID experiment of each individual species, there was a systematic decrease in retention time as oxygen was added to the unsaturated acyl chain (22:6) in the form of hydroxide or peroxide, and as the unsaturated acyl chain was truncated to a shorter chain and terminated with aldehyde or carboxylic acid. Fig. 2 shows the CID spectra of (a) standard 18:0/22:6-PA species (peak #8 of Fig. 1) along with (b–g) CID of six Ox-PA species (peaks #9–13). The CID spectra of the original PA standard in Fig. 2a shows typical fragment ions marked with the numbers in which commonly found fragment ions for all of the Ox-PA molecules are marked without indicating each m/z value in the spectra (fragment ions (1), (3), and (4)), however the type of fragment ion with corresponding m/z value is described in the figure caption. For the same type of fragment ions with different m/z values according to oxidation, the individual *m/z* value (fragment ions (2), (5), and (6)) was marked in each MS spectra. For instance, fragment ions (1) and (2) in Fig. 2a represent the free carboxylate ions, $[RCOO]^-$, of the acyl chain from sn-1 and sn-2, respectively, but the m/z value of the $[R_2COO]^-$ ion varies upon hydroxylation, peroxidation, and chain breakage while the *m/z* value of $[R_1COO]^-$ is fixed at *m/z* 283.4. Fragment ions (3) and (4) represent the loss of the sn-2 acyl chain (R_2) in the form of a carboxylate ($[M\text{-}H\text{-}R_2COOH]^-$, *m/z* 419.2) and ketene ($[M{-}H{-}R_2'CH{=}C{=}O]^-$, *m/z* 437.3), respectively. However, fragment ions (5) and (6) in Fig. 2a–e are from the dissociation of the R_1 acyl chain as $[M{-}H{-}R_1COOH]^-$ and $[M{-}H{-}R_1'CH{=}C{=}O]^-$, and the *m/z* values of both fragment ions vary upon oxidation at the R_2 chain. The CID spectra of nLC peak # 9 (*m/z* 763.6, 29.8 min) from the BPC in Fig. 1b is shown in Fig. 2b, which represents similar fragmentation patterns observed with that of the original PA standard, but shows the loss of water from the R_2 acyl chain marked with fragment ions (2)-H_2O (*m/z* 325.3, $[R_2COO{-}H_2O]^-$) and (7) (*m/z* 745.5, $[M{-}H{-}H_2O]^-$). The precursor ion of Fig. 2b is a result of the addition of an oxygen atom to the R_2 acyl chain in the form of hydroxide or ketone, though they cannot be resolved from the current MS spectra. Therefore, the precursor ion of Fig. 2b is expressed as 18:0/22:6 + O-PA.

The addition of two oxygen atoms to the unsaturated acyl chain may result in a combination, such as one peroxide (expressed as 18:0/22:6 + OO in Table 1) or two hydroxides (or ketones) (expressed as 18:0/22:6 + 2O). The addition of a peroxide can be

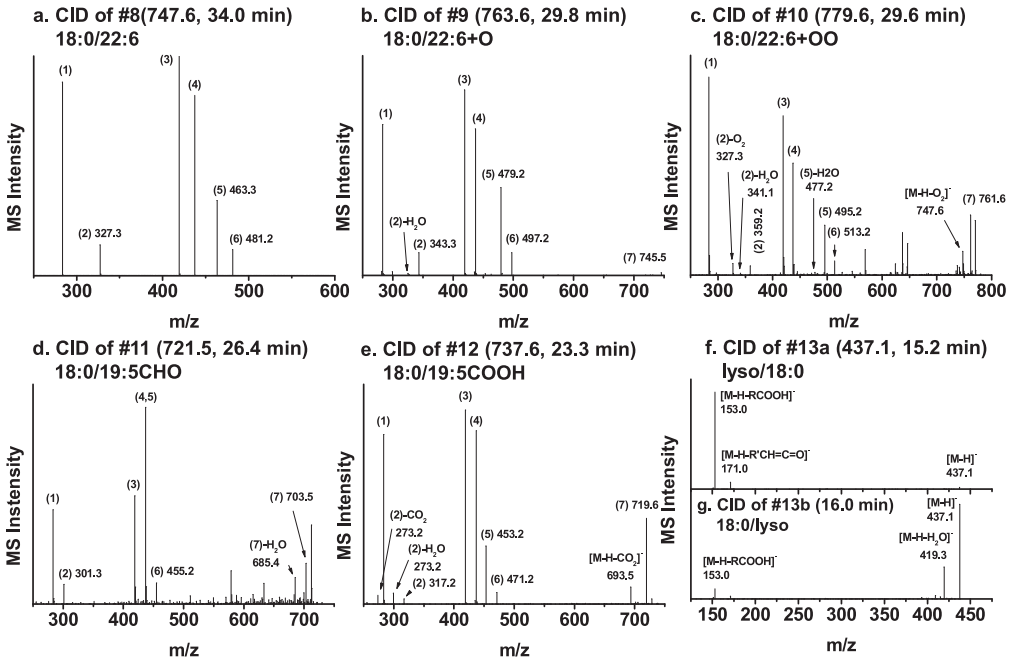

Fig. 2. Data dependent CID spectra of Ox-PA species shown in Fig. 1b: CIDs of peak (a) 8 (*m/z* 747.6, 34.0 min), (b) 9 (763.6, 29.8 min), (c) 10 (779.6, 29.6 min), (d) 11 (721.5, 26.4 min), (e) 12 (737.6, 23.3 min), (f) 13a (437.1, 15.2 min) and (g) 13b (437.1, 16.0 min). Spectra (a)–(e) show the same fragment ions as (1) $[R_1COO]^-$, *m/z* 283.4, (3) $[M-H-R_2COOH]^-$, *m/z* 419.2, and (4) $[M-H-R_2'CH=C=O]^-$, *m/z* 437.3. The same type of fragment ions with varied *m/z* values for each spectra are as (2) $[R_2COO]^-$, (5) $[M-H-R_1COOH]^-$, (6) $[M-H-R_1'CH=C=O]^-$, and (7) $[M-H-H_2O]^-$.

distinguished from the addition of two hydroxides or ketones by an increase in the retention time (29.6 min vs. 27.9 min in Table 1) and by the presence of the fragment ions in Fig. 2c showing the loss of O_2 from both the parent ion as $[M-H-O_2]^-$ at *m/z* 747.6 and the free carboxylate ion as $[(2)-O_2]^-$ at *m/z* 327.3, while other fragment ion patterns are similar to those in Fig. 2b. The latter two types of fragment ions were not observed in the CID spectra of 18:0/22:6 + 2O species, which was not shown, but the list of fragment ions are shown in Table 1.

The formation of short chain products by oxidation of the unsaturated acyl chain was systematically observed with a sequential truncation of three carbon chains from the R_2 chain (from 22 carbons to 19, 16, 13, 10, and 7) and with the modification of terminal carbon into aldehyde or carboxylic acid, as listed in Table 1. Fig. 2d and e shows the CID spectra of peak # 11 (26.4 min, *m/z* 721.5) and 12 (23.3 min, *m/z* 737.6) in Fig. 1b, respectively. While the CID spectra of a short chain product in Fig. 2d shows fragment ion patterns similar to those of un-oxidized molecules, except the presence of a fragment ion resulting from an additional loss of a water molecule from the fragment ion (7) as marked with (7)-H_2O, Fig. 2e exhibits unique fragment ions formed by the dissociation of CO_2 from both the parent ion and free carboxylic ion as $[M-H-CO_2]^-$ (*m/z* 693.5) and $[R_2COO-CO_2]^-$ (*m/z* 273.2), respectively. The former evidence represents the presence of a terminal aldehyde marked as 18:0/19:5CHO-PA, but the latter supports a terminal carboxylic acid as 18:0/19:5COOH-PA.

The formation of lysophosphatidic acid (LPA) from oxidation was confirmed with the CID spectra of the two regioisomers (lyso/18:0-PA and 18:0/lyso-PA in Fig. 2f and g, respectively). Since the regioisomers of the lyso PL species retain differently in reversed phase resins (C18), their geometrical differences can be clearly identified by the CID spectra in which the relative intensity of the two fragment ions, $[M-H-RCOOH]^-/[M-H]^-$, is predominantly large for lyso/18:0-PA, while a reversed ratio is observed for 18:0/lyso-PA as reported in an earlier work [32]. Since the acyl chain 18:0 was present at the sn-1 position of the original standard PA molecule, the presence of the lyso/18:0-PA may support that the exchange of an acyl chain in regioisomers can be possibly made during oxidation. This will be explained later with the LPA species identified from Ox-LDL.

When hydroxylation of the unsaturated acyl chain occurs, a number of possible isobaric species depending on the location of hydroxylation can be produced. Fig. 3 shows the three extracted ion chromatograms (EICs) of precursor ions ($[M-H]^-$) with *m/z* values of (a) 763.6, (b) 795.6, and (c) 827.7 that are from the addition of one, three, and five oxygen atoms to 18:0/22:6-PA, respectively. The top chromatogram is extracted from Fig. 1b for ion species having *m/z* 763.6 and the broad peak is attributed to the retention of isobaric 18:0/22:6 + O-PA species of which molecular structures can be confirmed from the CID spectra. For example, CID spectra of

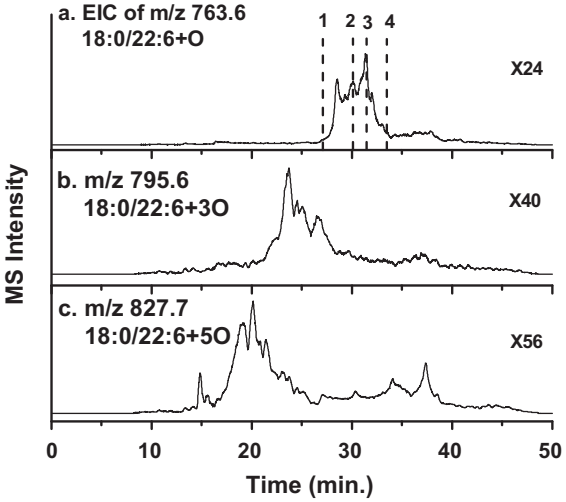

Fig. 3. Extracted ion chromatograms (EICs) of isobaric Ox-PA species, $[M-H]^-$, having *m/z* values of (a) 763.6, (b) 795.6, and (c) 827.7 representing the addition of one, three, and five oxygen atoms to 18:0/22:6-PA, respectively. CID spectra obtained at time slices of 1–4 represent the different locations of hydroxylation.

Table 1
List of identified Ox-PA species that were oxidatively-modified from standard 18:0/22:6-PA and the *m*/*z* value of the characteristic fragment ion during the nLC–ESI–MS/MS experiment.

R_2 species	Oxidation time			t_r	$[M-H]^-$	$[M-H-n(H_2O)]^-$	$[M-H-O_2]^-$	$[M-H-CO_2]^-$	$[R_2COO]^-$	$[M-H-R_1COOH]^-$	$[M-H-R_1' CH=C=O]^-$
	ctrl	1 h	2 h						/—$n(H_2O)$, —O_2, —CO_2	/—n(H_2O), —O_2, —CO_2	
22:6	O	O	O	34.0	747.6	–	–	–	327.3	463.1	481.1
22:6+O	O	O	O	29.8	763.5	745.6	–	–	343.2/325.2	497.2	497.2
22:6+2O	O	O	O	27.9	779.5	761.5	–	–	359.2/341.2	495.2	513.2
22:6+OO	O	O	O	29.6	779.6	761.6, 743.4	747.6	–	359.3/327.1	495.2	513.2
22:6+3O		O	O	24.1	795.6	777.6, 759.5	–	–	375.2/357.1, 339.2	511.2/493.2	529.1
22:6+O,OO		O	O	25.8	795.6	777.6, 759.5	736.7	–	375.2/343.2	511.2/493.2	529.2
22:6+4O		O	O	22.9	811.6	793.6, 775.6	–	–	391.2/373.2, 355.3, 337.3	527.2/509.2, 491.2	545.3
22:6+4O(OO)		O	O	24.8	811.6	793.6, 775.5	779.6	–	391.1/373.2, 355.2	527.2/509.3	545.1
22:6+5O		O	O	19.7	827.7	809.4, 791.5	–	–	407.1/389.2, 371.2	543.1/525.1, 507.2	561.4
22:6+5O(OO)		O		21.6	827.7	809.5, 791.5	783.6	–	407.1/389.2, 371.2	543.1/525.2, 507.3	561.4
22:6+6O		O	O	16.5	843.6	825.6, 807.6	–	–	423.2/408.2, 387.1, 369.2	559.2/541.2, 523.3	577.3
22:6+6O(OO)			O	19.7	843.6	825.6, 807.5	811.6	–	423.2/408.2, 387.2, 391.2	559.2/541.2	577.3
18:0/lyso		O	O	16.0	437.3	419.2	–	–	-	153.0	171.0
lyso/18:0			O	15.2	437.3	419.2	–	–	-	153.0	171.0
lyso/22:6		O	O	15.5	481.4	–	–	–	-	153.0	171.0
19:5CHO			O	26.4	721.5	703.5	–	–	301.3/283.4	437.1	455.2
19:5CHO+O		O	O	17.0	737.6	719.5, 701.4	705.5	–	317.1/299.3, 281.3	453.1	471.2
19:5COOH			O	23.3	737.6	719.5	–	693.6	317.1/299.3	453.1	471.2
19:5COOH+4O		O	O	16.4	801.5	783.6, 765.5	–	757.4	381.1/337.1	517.3/479.3	535.4
19:5COOH+7O(OO)			O	15.2	859.5	841.5, 823.5, 805.6	827.6	815.6	439.2/421.3, 403.2, 407.1	575.2/557.2	593.1
16:4CHO		O	O	23.7	681.5	663.5	–	–	261.4	397.3	415.2
16:4CHO+O		O	O	16.8	697.5	679.5	–	–	277.3/259.3, 241.2	413.1	431.1
16:4COOH		O	O	21.9	697.3	679.5	–	653.5	277.3/243.3	413.2	431.2
16:4COOH+O		O	O	16.6	713.5	695.5	–	669.5	275.3	429.1	447.1
16:4COOH+OO,O			O	16.2	745.5	727.5, 709.5	713.5	701.5	325.3/281.4	461.1	479.1
16:4COOH+4O		O	O	15.3	761.5	743.5, 725.3	–	–	341.2/297.4	477.2	419.2
16:4COOH+4O(OO)			O	16.1	761.5	743.5	729.5	717.5	341.3/297.4	477.2	495.1
16:4COOH+5O(OO)		O	O	16.5	777.5	759.5, 741.5	745.5	733.6	357.2/339.1, 313.1	493.2/475.2	511.2
16:4COOH+6O(OO)		O	O	16.3	793.5	775.4, 757.4	761.4	749.7	373.1/355.1, 329.3	509.2/491.1	527.3
16:4COOH+4OO		O	O	15.9	825.6	807.5, 789.5	793.6	781.5	405.2/387.2, 369.2	541.2/523.2, 509.3	559.2
13:3CHO		O	O	22.3	641.6	623.4	–	–	221.2	357.2	375.0
13:3CHO+O			O	16.6	657.4	639.4	–	–	237.2/219.2	373.1/355.1	391.1
13:3COOH		O	O	20.8	657.4	639.4	–	613.4	237.2/193.1, 219.2	373.1/355.1	391.1
13:3CHO+2O			O	15.8	673.5	655.4	–	–	253.4/235.3	389.2	407.2
13:3CHO+OO			O	16.4	673.5	655.4	–	–	253.4/221.2	389.2/371.2	407.2
13:3COOH+O		O	O	16.5	673.5	655.5, 637.5	–	629.4	253.3/209.1	389.2	407.3
13:3COOH+2O		O	O	15.3	689.5	671.5, 653.4	–	645.5	269.2/251.3, 233.2	405.1/387.1	423.1
13:3COOH+OO			O	16.3	689.5	671.6	645.5	645.4	269.2/235.3	405.0	–
10:2CHO		O	O	21.1	601.5	583.4	–	–	181.2	317.2	335.0
10:2CHO+O			O	16.4	617.5	599.5, 581.5	–	–	197.1	333.1/315.1	351.0
10:2COOH		O	O	19.9	617.5	599.4	–	573.5	197.1/179.1	333.2/315.2	351.1
10:2COOH+O		O	O	16.3	633.4	615.4	–	589.4	213.2/195.1	349.3/331.0	367.1
10:2CHO+OO,O			O	16.2	649.4	631.5, 613.4	617.4	–	229.2/211.1	365.3/333.2	383.1
10:2COOH+2O			O	15.2	649.4	631.4	–	605.4	229.2/211.1	365.1/347.1	383.1
10:2COOH+OO			O	16.2	649.4	631.4, 613.4	617.4	613.4	229.1/211.1	365.1/347.1	383.1
7:1CHO			O	20.1	561.5	543.4	–	–	-	277.6	295.3
7:1CHO+O			O	16.3	577.4	559.3, 541.4	–	–	-	293.3	311.3
7:1COOH		O	O	19.0	577.4	559.3	–	533.5	-	293.2	311.3
7:1COOH+O			O	16.1	593.5	575.3	–	549.4	173.2	309.2	327.2
7:1COOH+OO		O	O	15.9	609.5	591.3	577.3	565.3	159.4	325.3/307.9	–

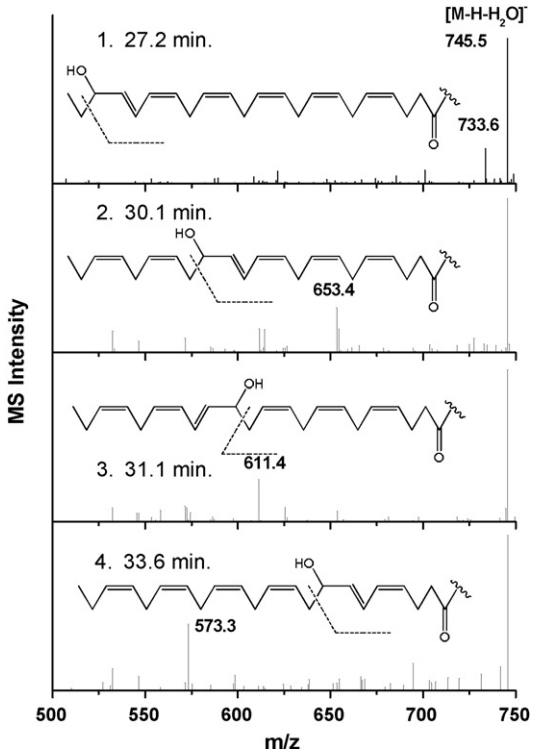

Fig. 4. CID spectra obtained at time slices of 1–4 in Fig. 3 represent the single hydroxylation located from an outer most to inner double bond of the R2 chain from top to bottom.

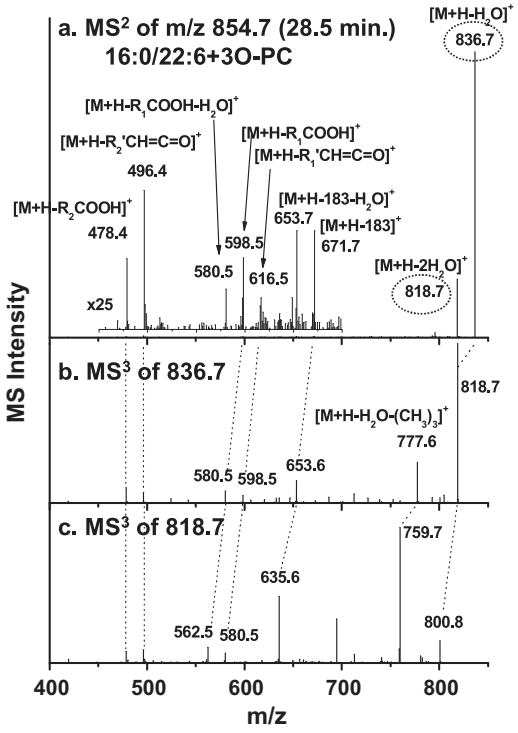

Fig. 6. (a) MS^2 fragment ion spectra of m/z 854.7 (at 28.5 min of nLC–ESI–MS^n run of Ox-PC products), (b) MS^3 spectra of m/z 836.7 ($[M+H—H_2O]^+$), and (c) MS^3 spectra of m/z 818.7 ($[M+H–2H_2O]^+$).

parent ions marked at time slices of 1–4 in Fig. 3a are plotted in Fig. 4, presuming four different locations of hydroxylation from the outer most to the inner double bond of the R2 chain. The position of a hydroxide can be confirmed from each fragment ion peak at m/z 733.6, 653.4, 611.4, and 573.3, which results from the cleavage of the carbon chain next to the hydroxylation at carbon number 3, 9, 11, and 15 (from the chain terminal), respectively, as marked with a dotted line of a presumed cleavage site. As hydroxylation occurs toward an inner double bond, hydrophobic interaction of the acyl chain with the C18 stationary phase becomes stronger, resulting in the increase in retention time marked in Fig. 4. While the isobaric species of a single hydroxylation can be readily identified from the CID spectra, the relative amount of the Ox-PA species containing more oxygen atoms significantly decreases as shown with an increase in magnification scales of the EICs (from 24 times magnification to (b) 40 and (c) 56 times) in Fig. 3. In addition, the retention time of a higher degree of hydroxylation decreases.

Examination of the oxidized PG products (oxidized from 18:0/22:6-PG, LC peak # 17 shown in Fig. 1c) with nLC–ESI–MS–MS reveals similar oxidation patterns observed for Ox-PAs, however separation of these species has slightly better resolution that made it possible to clearly identify the three interesting isobaric species of short chain products. Fig. 5 shows the CID spectra of precursor ions from LC peaks # 14–16 marked in Fig. 1c. The three precursor ions have the same m/z 835.8 but slightly different retention times (18.3, 18.9, and 19.1 min for Fig. 5a–c, respectively, based on the retention time of each CID spectra obtained) that can be expected to have six oxygen atoms added to the truncated sn-2 acyl chain (from 22:6 to 16:4). While the CID spectra of the three precursor ions in Figure 5 exhibit the same fragment ions for (1) $[R_1COO]^-$ at m/z 283.4, (2) $[R_2COO]^-$ at 341.2,

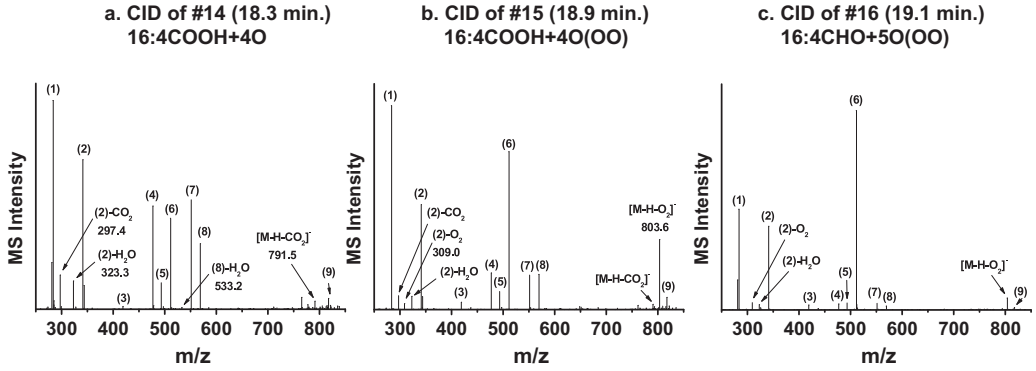

Fig. 5. Comparison of CID spectra of the three isobaric species of which parent ions are the peaks (a) 14, (b) 15, and (c) 16 marked in Fig. 1c. The three CID spectra exhibit the common fragment ions (fragment ions (1)–(9)) except the fragment ions formed by the loss of CO_2 and H_2O from parent ion and free carboxylate ion of sn-2 acyl chain. The common fragment ions: (1) m/z 283.4 $[R_1COO]^-$, (2) 341.2 $[R_2COO]^-$, (3) 419.3 $[M—H—74—R_2COOH]^-$, (4) 477.3 $[M—H—74—R_1COOH]^-$, (5) 493.3 $[M—H—R_2COOH]^-$, (6) 511.3 $[M—H—R_2'CH=C=O]^-$, (7) 551.3 $[M—H—R_1COOH]^-$, (8) 569.3 $[M—H—R_1'CH=C=O]^-$, (9) 817.7 $[M—H—H_2O]^-$.

Table 2
List of identified PL and Ox-PL species from LDL standard materials before and after oxidative modification during the (a) negative and (b) positive ion modes of nLC–ESI–MS/MS experiments.

m/z	Species	Sample Control/OxLDL	*m/z*	Species	Sample Control/OxLDL	*m/z*	Species	Sample Control/OxLDL
(a) Negative ion mode								
	PA		696.4	18:2/17:1CHO	/O	826.7	19:5CHO + OO/18:0	/O
696.6	16:0/20:3	O/	775.7	20:0/19:0COOH	/O	824.7	19:5CHO + OO/18:1	/O
534.4	12:0/12:0	/O	820.7	20:2COOH + 2OO/18:0	/O	830.6	20:4CHO + O&OO/16:0	/O
750.6	16:0/24:4	/O	508.3	16:0/4:0COOH	O/O	830.6	20:4COOH + OO/16:0	/O
722.6	18:0/20:4	/O	508.4	18:0/2:0COOH	O/O	857.6	20:4COOH + OO/18:1	/O
616.6	14:1/16:0	O/O		**PG**		840.6	20:5 + O&OO/18:1	/O
726.6	16:0/22:2	O/O	802.6	18:1/20:0	O/	812.7	20:5CHO + OO/16:0	/O
698.5	18:0/18:2	O/O	796.7	22:4/16:0	O/	824.7	20:6 + OO/16:0	/O
696.5	18:0/18:3	O/O	820.6	22:6/18:0	O/	856.6	21:3CHO + OO/18:0	/O
696.3	18:1/18:2	O/O	714.6	18:2/14:1	/O		**PI**	
694.5	18:2/18:2	O/O	790.6	20:6/18:1	/O	807.6	16:0/16:1	O/
722.6	20:4/18:0	O/O	820.7	24:5/16:1	/O	885.7	18:0/20:4	O/
746.5	20:4/20:2	O/O	746.6	18:1/16:0	O/O	887.6	20:3/18:0	O/
410.3	lyso/16:0	O/O	744.6	18:1/16:1	O/O	859.6	16:0/20:3	/O
410.4	16:0/lyso	O/O	774.6	18:1/18:0	O/O	857.6	16:0/20:4	/O
437.4	lyso/18:0	O/O	772.7	18:1/18:1	O/O	911.6	18:0/22:5	/O
433.3	18:2/lyso	O/O	800.6	18:1/20:1	O/O	885.6	18:1/20:3	/O
481.3	22:6/lyso	O/O	796.6	18:1/20:3	O/O	883.6	20:5/18:0	/O
743.1	16:0/22:2 + O	O/	744.7	18:2/16:0	O/O	809.6	16:0/16:0	O/O
437.2	18:0/lyso	/O	772.6	18:2/18:0	O/O	837.6	16:0/18:0	O/O
435.9	lyso/18:1	/O	770.7	18:2/18:1	O/O	835.7	16:0/18:1	O/O
435.7	18:1/lyso	/O	768.7	18:2/18:2	O/O	833.6	16:0/18:2	O/O
465.4	20:0/lyso	/O	794.6	18:2/20:3	O/O	807.6	16:1/16:0	O/O
457.3	20:4/lyso	/O	772.7	20:1/16:1	O/O	837.7	18:0/16:0	O/O
481.3	lyso/22:6	/O	800.6	20:1/18:1	O/O	865.6	18:0/18:0	O/O
671.2	13:2CHO + OO/18:2	/O	766.6	20:4/16:1	O/O	863.7	18:0/18:1	O/O
466.3	14:0/3:0COOH	/O	796.6	20:4/18:0	O/O	861.7	18:0/18:2	O/O
698.4	14:3COOH + OO/18:2	/O	824.7	20:4/20:0	O/O	887.7	18:0/20:3	O/O
697.5	15:0CHO/20:3	/O	822.7	20:4/20:1	O/O	883.6	18:0/20:5	O/O
464.3	16:0/2:0CHO	/O	818.7	22:6/18:1	O/O	913.7	18:0/22:4	O/O
480.4	16:0/2:0COOH	/O	846.6	22:6/20:1	O/O	909.6	18:0/22:6	O/O
494.3	16:0/3:0COOH	/O	480.5	lyso/16:1	O/O	863.6	18:1/18:0	O/O
670.4	16:0/16:3COOH	/O	480.4	16:1/lyso	O/O	861.6	18:1/18:1	O/O
744.6	16:0/20:2COOH + O	/O	508.4	18:1/lyso	O/O	859.6	18:1/18:2	O/O
742.6	16:0/20:3CHO + OO	/O	538.4	lyso/20:0	O/O	883.6	18:1/20:4	O/O
707.7	16:0/16:1COOH + OO	/O	538.4	20:0/lyso	O/O	833.6	18:2/16:0	O/O
686.6	16:0/18:1CHO	/O	508.3	lyso/18:1	/O	885.6	20:4/18:0	O/O
736.7	16:0/22:5 + O	/O	530.4	20:4/lyso	/O	883.6	20:4/18:1	O/O
711.6	16:0/19:4COOH	/O	528.3	lyso/20:5	/O	901.6	20:5/20:5	O/O
692.7	17:2CHO/18:3	/O	554.3	lyso/22:6	/O	909.6	22:6/18:0	O/O
598.3	18:0/10:3CHO	/O	732.6	10:4COOH + O&OO/18:1	/O	816.6	18:0/14:3CHO	O/
699.5	18:0/16:3CHO + O	/O	750.6	12:3COOH + 4O(OO)/16:0	/O	599.4	lyso/18:0	/O
522.4	18:0/3:0COOH	/O	593.4	14:1/6:2COOH + O	/O	599.5	18:0/lyso	/O
492.4	18:0/2:0CHO	/O	749.7	14:1COOH + OO/16:1	/O	882.6	16:0/16:2COOH + O&OO	/O
731.4	18:0/17:2CHO + 2O	/O	779.6	14:3COOH + 4O(OO)/16:0	/O	890.8	16:0/19:3COOH + O	/O
763.7	18:0/22:6 + O	/O	775.7	14:5COOH + 4O(OO)/16:0	/O	910.6	18:0/16:2COOH + O&OO	/O
739.6	18:0/20:3CHO	/O	774.7	15:5CHO + 4O(OO)/16:0	/O	885.6	18:0/18:5COOH	/O
520.4	18:1/3:0COOH	/O	820.6	16:3CHO + 2OO/18:0	/O	889.6	18:0/19:2CHO	/O
506.4	18:1/2:0COOH	/O	790.6	16:4CHO + 4O(OO)/16:0	/O	901.6	18:0/20:3CHO	/O
490.4	18:1/2:0CHO	/O	814.6	16:5CHO + 4O(OO)18:1	/O	706.7	18:1/5:2COOH	/O
761.7	18:1/22:6 + O	/O	816.8	17:3CHO + O&OO/18:1	/O	901.6	20:3CHO/18:0	/O
518.4	18:2/3:0COOH	/O	818.6	17:3COOH + OO/18:0	/O		**PS**	
504.4	18:2/2:0COOH	/O	787.7	17:4COOH + OO/16:0	/O	496.4	16:0/lyso	O/O
488.4	18:2/2:0CHO	/O	820.6	19:1COOH + O/16:1	/O	494.4	16:1/lyso	/O
(b) Positive ion mode								
	PC		496.4	16:0/lyso	O/O	796.8	16:0/20:5 + O	/O
732.8	14:0/18:1	O/	494.6	lyso/16:1	O/O	812.8	16:0/20:5 + OO	/O
788.8	16:0/20:1	O/	524.5	lyso/18:0	O/O	846.8	16:0/21:2CHO + 2O	/O
790.8	18:0/18:0	O/	524.7	18:0/lyso	O/O	810.8	16:0/21:4CHO	/O
754.8	14:0/20:4	O/O	522.5	lyso/18:1	O/O	808.8	16:0/21:5CHO	/O
734.9	16:0/16:0	O/O	522.3	18:1/lyso	O/O	638.6	16:0/6:1CHO + OO	/O
732.8	16:0/16:1	O/O	520.5	lyso/18:2	O/O	636.6	16:0/6:2CHO + OO	/O
762.7	16:0/18:0	O/O	520.5	18:2/lyso	O/O	622.6	16:0/7:0CHO	/O
758.9	16:0/18:2	O/O	568.4	lyso/22:6	O/O	666.6	16:0/8:1CHO + OO	/O
780.8	16:0/20:5	O/O	568.3	22:6/lyso	O/O	648.6	16:0/9:1CHO	/O
808.8	16:0/22:5	O/O	548.4	20:2/lyso	O/	676.6	16:0/9:3CHO + OO	/O
756.8	16:1/18:2	O/O	706.8	16:0/11:2COOH + O	O/	816.8	18:0/16:4CHO + O&OO	/O
782.9	16:1/20:3	O/O	788.8	16:0/19:1CHO	O/	818.8	18:0/18:2 + 2O	/O
778.8	16:1/20:5	O/O	622.6	18:0/5:0CHO	O/	802.8	18:0/18:2 + O	/O
806.9	16:1/22:5	O/O	678.7	18:0/7:2CHO + OO	O/	856.7	18:0/20:4CHO + OO	/O
762.9	18:0/16:0	O/O	732.8	18:1/13:0CHO	O/	856.7	18:0/20:4COOH + O	/O
788.9	18:0/18:1	O/O	440.5	12:0/lyso	/O	664.6	18:0/6:2CHO + OO	/O

Table 2 (*Continued*)

m/z	Species	Sample Control/OxLDL	*m/z*	Species	Sample Control/OxLDL	*m/z*	Species	Sample Control/OxLDL
786.9	18:0/18:2	O/O	468.5	14:0/lyso	/O	662.6	18:0/8:1CHO	/O
812.8	18:0/20:3	O/O	518.5	18:3/lyso	/O	656.5	18:0/8:4CHO	/O
810.8	18:0/20:4	O/O	552.4	lyso/20:0	/O	746.9	18:1/14:0CHO	/O
808.8	18:0/20:5	O/O	548.4	lyso/20:2	/O	814.8	18:1/17:3CHO + OO	/O
836.8	18:0/22:5	O/O	546.5	20:3/lyso	/O	792.8	18:1 + OO/16:0	/O
834.8	18:0/22:6	O/O	544.5	20:4/lyso	/O	796.8	20:4/16:1 + O	/O
760.9	18:1/16:0	O/O	542.4	lyso/20:5	/O	606.5	6:1CHO/16:0	/O
786.8	18:1/18:1	O/O	542.3	20:5/lyso	/O	650.5	16:0/8:1COOH	O/O
784.9	18:1/18:2	O/O	570.5	lyso/22:5	/O	836.8	18:0/21:5CHO	O/O
810.8	18:1/20:3	O/O	570.6	22:5/lyso	/O		**PE**	
806.8	18:1/20:5	O/O	718.7	16:0/11:4CHO + O&OO	/O	796.5	20:0/20:4	/O
836.8	18:1/22:4	O/O	774.8	16:0/16:3CHO + OO	/O	746.5	18:1/18:0	O/O
834.8	18:1/22:5	O/O	788.8	16:0/17:3CHO + 2O	/O	744.9	18:1/18:1	O/O
832.8	18:1/22:6	O/O	790.8	16:0/18:2 + 2O	/O	772.9	20:2/18:0	O/O
756.9	18:2/16:1	O/O	774.8	16:0/18:2 + O	/O	482.6	lyso/18:0	O/O
784.8	18:2/18:1	O/O	806.8	16:0/18:2 + O&OO	/O	482.5	18:0/lyso	O/O
782.8	18:2/18:2	O/O	852.7	16:0/18:2COOH + 4O(OO)	/O	480.5	18:1/lyso	O/O
756.8	18:3/16:0	O/O	864.7	16:0/20:3 + 5O(OO)	/O	510.5	lyso/20:0	O/O
808.8	18:3/20:2	O/O	814.8	16:0/20:3CHO + O	/O	510.5	20:0/lyso	O/O
813.8	20:0/18:2	O/O	830.7	16:0/20:3COOH + O	/O	526.5	lyso/22:6	O/O
838.8	20:0/20:4	O/O	828.7	16:0/20:4CHO + 2O	/O	480.6	lyso/18:1	/O
780.9	20:4/16:1	O/O	828.8	16:0/20:4CHO + OO	/O	508.5	lyso/20:1	/O
496.5	lyso/16:0	O/O	844.7	16:0/20:5 + 4O(OO)	/O	502.0	20:4/lyso	/O

(3) $[M–H–74–R_2COOH]^-$ at 419.3, (4) $[M–H–74–R_1COOH]^-$ at 477.3, (5) $[M–H–R_2COOH]^-$ at 493.3, (6) $[M—H—R_2'CH=C=O]^-$ at 511.3, (7) $[M—H—R_1COOH]^-$ at 551.3, (8) $[M—H—R_1'CH=C=O]^-$ at 569.3, and (9) $[M—H—H_2O]^-$ at 817.7, the molecular structure of the precursor ions 14–16 can be differentiated by the presence of a few characteristic fragment ions formed from the loss of CO_2 and O_2. Both precursor ions in Fig. 5a and b contain fragment ions *m/z* 791.5 and 297.4 that are formed by the loss of CO_2 from the parent ion as $[M—H—CO_2]^-$ and from a free carboxylate ion as $[R_2COO—CO_2]^-$, respectively, supporting that the truncated acyl chain (16:4) was terminated with carboxylic acid and the remaining four double bonds were hydroxylated or oxidized in combination with the hydroxide and ketone forms (expressed as 16:4COOH + 4O). However, Fig. 5b contains additional fragment ions m/z 803.6 and 309.0 that were generated by the loss of O_2 from the parent ion as $[M—H—O_2]^-$ and from the free carboxylate ion as $[R_2COO—O_2]^-$, respectively, supporting that there is at least one peroxide added (expressed as 16:4COOH + 4O(OO)). Another interesting combination is shown in Fig. 5c, where fragment ions formed by the loss of CO_2 were not shown in comparison to those of Fig. 5b. This suggests that the terminal carbon was not carboxylated, resulting in the possibility of an aldehyde and five oxygen atoms added to the acyl chain, including one peroxide (expressed as 16:4CHO + 5O(OO)).

The Ox-PC species (oxidized from PC vesicles prepared with standard 16:0/22:6-PC) were examined by nLC–ESI–MS^n at the positive ion mode. While examining the oxidation patterns of the PC species, it was determined that MS^3 experiments were required for some oxidized species as characteristic fragment ions were not properly generated during the first CID experiment. Fig. 6 shows (a) the MS^2 spectra of the precursor ion with *m/z* 854.7 at 28.5 min (BPC not shown here) along with b–c) the two MS^3 spectra of the fragment ions *m/z* 836.7 and 818.7 from the first CID run representing consecutive loss of H_2O. During the first CID experiment, fragment ions formed from the loss of water molecules were prominent while the intensities of other typical fragment ions from the cleavage of the head group (−183 Da) and each acyl chain were very low (inset was magnified 25 folds). However, MS^3 experiments of the two prominent fragment ions showed the same type of fragment ions after the sequential loss of water molecules in Fig. 6b and c. A series of fragment ions showing a difference of 18 Da with the dotted line connection in Fig. 6, such as *m/z* 671.7 (in Fig. 6a), 653.6 (b), and 635.6 (c), represented the loss of the phosphocholine head group (183 Da). A similar observation was found with the two types of fragment ions showing the dissociation of the sn-1 acyl chain in the form of carboxylic acid or ketene, however m/z values of fragment ions from the loss of the sn-2 acyl chain (m/z 478.4 and 496.4) were fixed for all three CID experiments. Based on these spectra, three oxygen atoms were added to the sn-2 acyl chain as 16:0/22:6 + 3O-PC without a terminal carboxylic acid.

Based on the structural analysis of Ox-PL species from oxidative modification of PL vesicles, a standard LDL sample was oxidized for 2 h using a $CuSO_4$ solution and followed by extraction of Ox-PLs. The resulting PL mixtures from Ox-LDL were analyzed by nLC–ESI–MS^n in both the negative and positive ion modes. Fig. S1 of the Supporting Information shows the comparison of BPCs obtained with PL mixtures extracted from the control (standard LDL sample before oxidation) and Ox-LDL (2 h oxidation) in the negative ion mode. PLs and their oxidized species were characterized using LiPilot and the search results were confirmed manually. Table 2 lists the chain structures of PLs and Ox-PLs before and after oxidation. Most of the diacyl PL molecules identified from the control sample were also found in Ox-LDL, except some species that were not detected due to their relatively low concentrations. However, a few species, such as 12:0/12:0-PA, 16:0/24:4-PA, and 18:0/20:4-PA, were exclusively observed in Ox-LDL. A similar observation was also made with a number of lyso-PA species. Among newly found LPA species in Ox-LDL, those having an acyl chain with 18:0, 18:1, and 20:4 can be expected from the dissociation of an acyl chain from PA molecules. However, it cannot be assumed that 20:0/lyso-PA and lyso/22:6-PA originate from the identified list of PA molecules since PA species with any of these acyl chains (20:0 and 22:6) were not found in the control LDL sample. These can be presumed that a polar head group of other PL molecules (PG, PI, and PC having these type of acyl chains), including LPL, was substituted with hydrogen to generate PA and LPA species. Moreover, since the acyl chain 22:6 among identified PG lists was only in the sn-1 position, the presence of lyso/22:6-PG in the Ox-LDL supported that the exchange of acyl chain positions (between sn-1 and sn-2) of LPG during oxidation may occur, as observed in Fig. 2f. Similar observations were made from species with other head groups, such as 20:3/lyso-PC, 20:5/lyso-PC, and 22:5/lyso-PC. For the case of PAs, 40 Ox-PA species, including the addition of oxygen, acyl chain truncation, and formation of LPA, were identified while the control LDL sample exhibited only 14 PAs. For the Ox-PAs and Ox-PCs identified in

Table 3
Number of identified PL and Ox-PL species before and after oxidative modification of standard LDL materials.

	Std. LDL PLs/Ox-PLs	Ox-LDL PLs/Ox-PLs	Unique species PLs/Ox-PLs
PA	14/3	16/40	17/41
PG	27/–	27/27	30/27
PI	25/1	27/10	30/11
PS	1/–	1/1	1/1
PC	50/7	46/50	49/56
PE	9/–	10/3	10/3
Sum	137	258	276

this study, most oxidation occurred at the sn-2 acyl chain position. However, the Ox-PG molecules showed opposite results as sn-1 acyl chains of most PGs were highly unsaturated.

Supplementary data associated with this article can be found, in the online version, at http://dx.doi.org/10.1016/j.chroma.2013.02.086.

While most PL species were significantly oxidized, Ox-PE species were not detected much in this experiment. Since PE molecules during the CID experiment in general exhibited an intense fragment ion peak originating from the loss of the phosphoethanolamine head group ($HPO_4(CH_2)_2NH_3$, 141 amu), the relative intensities of other characteristic fragment ion peaks, such as from the loss of the acyl chain in the form of ketene or carboxylic acid, were very low [33]. This resulted in a substantial decrease of the peak intensity of those fragment ions from Ox-PE molecules and led to a failure in identification. Moreover, the PS species was rarely found in LDL as previously observed in our earlier studies with human plasma [29,32]. Due to the diversity of the PC molecular structures, 50 out of 137 PLs were observed in the control LDL sample, leading to the identification of 46 PCs and 50 Ox-PCs as listed in Table 3. In total, 258 species, including 131 oxidized species, were observed from Ox-LDL, while 137 PL species were identified from the standard LDL.

4. Conclusions

In this study, molecular structures of oxidized phospholipids have been systematically examined by nLC–ESI–MS^n analysis of various Ox-PLs produced from the oxidation of vesicles made with each PL standard: 18:0/22:6-PA, 18:0/22:6-PG, 16:0/22:6-PC. The pattern analysis of oxidized products was applied to the profiling of Ox-PLs of LDL particles that were oxidatively modified. The current nanoflow LC separation clearly resolved various Ox-PL products from hydroxylation or hydroperoxylation at the unsaturated acyl chain, truncation of acyl chain with the formation of terminal aldehyde or carboxylic acid, and cleavage of an acyl chain to produce a lyso PL species along with the structural determination from tandem MS analysis. It is presumed that the location of an acyl chain in LPL can be exchanged between sn-1 and sn-2 positions during the cleavage of an acyl chain, and the polar head group of PL molecules can be dissociated during oxidation to form PA species. It demonstrates that the current study can be applied in the future for the comprehensive analysis of Ox-PL species in lipoprotein particles from human plasma in relation to age-related cardiovascular diseases, which can be helpful in understanding the relationship of Ox-PLs with the developmental stage of such diseases.

Acknowledgements

This study was supported by a grant (No. 2010-0014046) from the National Research Foundation (NRF) of Korea funded by the Korean Government (MEST).

References

[1] S. Parthasarathy, A. Raghavamenon, M. Omar, G. Garelnabi, N. Santanam, Free Radicals and Antioxidant Protocols, Springer, New York, 2010.
[2] J.L. Witztum, J. Clin. Invest. 88 (1991) 1785.
[3] M. Navab, S.Y. Hama, S.T. Ready, C.J. Ng, B.J. Van Lenten, H. Laks, A.M. Fogelman, Lipidology 13 (2002) 363.
[4] S. Ehara, M. Ueda, T. Naruko, K. Haze, A. Itoh, M. Otsuka, R. Komatsu, T. Matsuo, H. Itabe, T. Takano, Y. Tsukamoto, M. Yoshiyama, K. Takeuchi, J. Yoshikawa, A.E. Becker, Circulation 103 (2001) 1955.
[5] J. Adachi, M. Asano, N. Yoshioka, H. Nushida, Y. Ueno, Kobe J. Med. Sci. 52 (2006) 127.
[6] J. Adachi, N. Yoshioka, R. Funae, H. Nushiba, M. Asano, Y. Ueno, J. Chromatogr. B Anal. Technol. Biomed. Life Sci. 806 (2004) 41.
[7] J. Adachi, N. Yoshioka, R. Funae, Y. Nagasaki, H. Nushida, M. Asano, Y. Ueno, Chem. Phys. Lipids 130 (2004) 46.
[8] F.M. Megli, K. Sabatini, FEBS Lett. 573 (2004) 68.
[9] F.M. Megli, L. Russo, E. Conte, Biochim. Biophys. Acta 1788 (2009) 371.
[10] A.D. Watson, N. Leitinger, M. Navab, K.F. Faull, S. Hörkkö, J.L. Witztum, W. Palinski, D. Schwenke, R.G. Salomon, W. Sha, G. Subbanagounder, A.M. Fogelman, J.A. Berliner, J. Biol. Chem. 272 (1997) 13597.
[11] M.R.M. Domingues, A. Reis, P. Domingues, Chem. Phys. Lipids 156 (2008) 1.
[12] V.B. O'Donnell, Biochim. Biophys. Acta 1811 (2011) 818.
[13] X. Han, R.W. Gross, J. Am. Chem. Soc. 118 (1996) 451.
[14] F.F. Hsu, J. Turk, J. Am. Soc. Mass Spectrom. 14 (2003) 352.
[15] C.M. Spickett, A.R. Pitt, A.J. Brown, Free Radic. Biol. Med. 25 (1998) 613.
[16] M. Ishida, T. Yamazaki, T. Houjou, M. Imagawa, A. Harada, K. Inoue, R. Taguchi, Rapid Commun. Mass Spectrom. 18 (2004) 2486.
[17] A. Reis, P. Domingues, A.J.V. Ferrer-Correaia, M.R.M. Domingues, J. Mass Spectrom. 39 (2004) 1513.
[18] K.A. Harrison, S.S. Davies, G.K. Marathe, T. McIntyre, S. Prescott, K.M. Reddy, J.R. Falck, R.C. Merphy, J. Mass Spectrom. 35 (2000) 224.
[19] H. Vitrac, M. Courrègelongue, M. Couturier, F. Collin, P. Thérond, S. Rémita, P. Peretti, D. Jore, M. Gardès-Albert, Can. J. Physiol. Pharmacol. 82 (2004) 153.
[20] A. Reis, M.R.M. Domingues, F.M.L. Amado, A.J.V. Ferrer-Correia, P. Domingues, Biomed. Chromatogr. 19 (2005) 129.
[21] X. Chen, W. Zhang, J. Laird, S.L. Hazen, R.G. Salomon, J. Lipid Res. 49 (2008) 832.
[22] C.M. Spickett, N. Rennie, H. Winter, L. Zambonin, L. Landi, A. Jerlich, R.J. Schaur, A.R. Pitt, Biochem. J 355 (2001) 449.
[23] A. Ravandi, S. Babaei, R. Leung, J.C. Monge, G. Hoppe, H. Hoff, H. Kamido, A. Kuksis, Lipids 39 (2004) 97.
[24] A. Reis, M.R.M. Domingues, F.M.L. Amado, A.J. Ferrer-Correia, P. Domingues, J. Chromatogr. B 855 (2007) 186.
[25] L.T. Morgan, C.P. Thomas, H. Kühn, V.B. O'Donnell, Biochem. J 431 (2010) 141.
[26] S.R. Clark, C.J. Guy, M.J. Scurr, P.R. Taylor, A.P. Kift-Morgan, V.J. Hammond, C.P. Thomas, B. Coles, W. Roberts, M. Eberl, S.A. Jones, N. Topley, S. Kotecha, V.B. O'Donnell, Blood 117 (2011) 2033.
[27] H. Kim, E. Ahn, M.H. Moon, Analyst 133 (2008) 1656.
[28] H.K. Min, S. Lim, B.C. Chung, M.H. Moon, Anal. Bioanal. Chem. 399 (2011) 823.
[29] J.Y. Lee, H.K. Min, D. Choi, M.H. Moon, J. Chromatogr. A 1217 (2010) 1660.
[30] S. Lim, S.K. Byeon, J.Y. Lee, M.H. Moon, J. Mass Spectrom. 47 (2012) 1004.
[31] C. Wu, Y. Peng, J. Chiu, Y. Ho, C. Chong, Y. Yang, M. Liu, J. Chromatogr. B 877 (2009) 3495.
[32] J.Y. Lee, H.K. Min, M.H. Moon, Anal. Bioanal. Chem. 400 (2011) 2953.
[33] H. Kim, H.K. Min, G. Kong, M.H. Moon, Anal. Bioanal. Chem. 393 (2009) 1649.